



Spectral-line Survey of the Region of Massive Star Formation W51e1/e2 in the 4 mm Wavelength Range

Sergei. V. Kalenskii¹ , Ralf I. Kaiser² , Per Bergman³, A. O. Henrik Olofsson³ , Kirill D. Degtyarev⁴, and Polina Golysheva^{1,5}¹ Lebedev Physical Institute, Astro Space Center, 84/32 Profsoyuznaya st., Moscow, GSP-7, 117997, Russia; kalensky@asc.rssi.ru² Department of Chemistry, University of Hawaii at Manoa, Honolulu, HI, 96822, USA³ Department of Space, Earth and Environment, Chalmers University of Technology, Onsala Space Observatory, SE-43992 Onsala, Sweden⁴ Moscow Institute of Physics and Technology, 9 Institutskiy per., Dolgoprudny, Moscow Region, 141700, Russia⁵ Sternberg Astronomical Institute, Moscow State University, Universitetsky pr., 13, Moscow 119234, Russia

Received 2022 February 11; revised 2022 March 28; accepted 2022 March 30; published 2022 June 8

Abstract

We present the results of a spectral-line survey of the W51e1/e2 star-forming region at 68–88 GHz. 79 molecules and their isotopologues were detected, from simple diatomic or triatomic molecules, such as SO, SiO, and CCH, to complex organic compounds, such as CH₃OCH₃ or CH₃COCH₃. A number of lines that are absent from the Lovas list of molecular lines observed in space were detected, and most of these were identified. A significant number of the detected molecules are typical for hot cores. These include the neutral molecules HCOOCH₃, CH₃CH₂OH, and CH₃COCH₃, which are currently believed to exist in the gas phase only in hot cores and shock-heated gas. In addition, vibrationally excited C₄H and HC₃N lines with upper-level energies of several hundred Kelvins were found. Such lines can arise only in hot gas with temperatures on the order of 100 K or higher. Apart from neutral molecules, various molecular ions were also detected. Some of these (HC¹⁸O⁺, H¹³CO⁺, and HCS⁺) usually exist in molecular clouds with high visual extinctions. Potential formation pathways of complex organic molecules and hydrocarbons, along with nitriles, are considered. These formation routes are first discussed in the context of laboratory experiments elucidating the synthesis of organic molecules in interstellar ices in cold molecular clouds, followed by sublimation into the gas phase in the hot core stage. Thereafter, we discuss the predominant formation of hydrocarbons and their nitriles in the gas phase through bimolecular neutral–neutral reactions.

Unified Astronomy Thesaurus concepts: [Interstellar medium \(847\)](#); [Pre-biotic astrochemistry \(2079\)](#); [Star forming regions \(1565\)](#)

Supporting material: machine-readable table

1. Introduction

Spectral-line surveys covering wide frequency bands are an effective tool for studying molecular clouds. Since multiple spectral lines fall within the ranges of such surveys, they allow us to fully investigate the molecular compositions of the studied sources and to explore the chemical processes taking place there. Surveys performed with high sensitivity make it possible to search for molecules previously undetected in space. For example, as a result of the survey of the dark cloud TMC-1, performed by Kaifu et al. (2004), 11 new molecules were discovered; in addition, using the spectra obtained in this survey, it was later possible to detect a 13-atom molecule, c-C₆H₅CN (benzonitrile; Kalenskii 2017; McGuire et al. 2018). In 2018, a new, more sensitive spectral survey of TMC-1 was launched, which was named GOTHAM (McGuire et al. 2020). As a result of this still-incomplete survey, about a dozen new molecules have been discovered, including two nitrile-group-functionalized polycyclic aromatic hydrocarbons, 1- and 2-cyanonaphthalene (C₁₀H₇CN; McGuire et al. 2021).

In addition to establishing the molecular compositions of cosmic sources, spectral surveys make it possible to explore their structures and physical parameters. For example, according to the results of the scanning the region of high-mass star formation closest to the Sun, OMC-1, three subregions were

identified, designated Ridge, Plateau, and Hot Core, and the basic physical parameters and molecular compositions of each of them were determined (Blake et al. 1987).

In 2010, the results of the spectral scanning of the regions of high-mass star formation DR21OH and W51e1/e2, in the 3 mm wavelength range, performed with the 20 m radio telescope of the Onsala Space Observatory (Sweden), were published (Kalenskii & Johansson 2010a, 2010b). In W51e1/e2, the emission of 105 molecules was detected, from simple diatomic or triatomic species, such as CO, CS, and HCN, up to complex organic compounds, such as CH₃OCH₃, CH₃COCH₃, or HCOOC₂H₅. A significant number of the detected molecules are typical for hot cores, for example, HCOOCH₃, CH₃CH₂OH, and CH₃COCH₃. In addition, lines of the vibrationally excited states of SiO, C₄H, HCN, 1-C₃H, HC₃N, CH₃CN, CH₃OH, H₂O, and SO₂ were detected, with upper-level excitation temperatures on the order of several hundred Kelvins. Such lines can occur only in hot gas with a temperature on the order of 100 K or higher. An interesting result was the possible detection of two molecules, MgCN and NaCN, which have so far been observed only in the atmospheres of evolved giant stars (Ziurys et al. 1995; Highberger et al. 2000). Further observations are needed to confirm or refute this detection. In addition, the stacked spectra suggest the existence of several molecules not yet discovered in space—HOCH₂COOH (glycolic acid), H₂SO₄ (sulfuric acid), gG'a-CH₃CHOHCH₂OH (propanediol), and 1-C₇H₂ (heptahexainylidene).⁶

Original content from this work may be used under the terms of the [Creative Commons Attribution 4.0 licence](#). Any further distribution of this work must maintain attribution to the author(s) and the title of the work, journal citation and DOI.

⁶ The possible detection of these molecules was not mentioned in Kalenskii & Johansson (2010b).

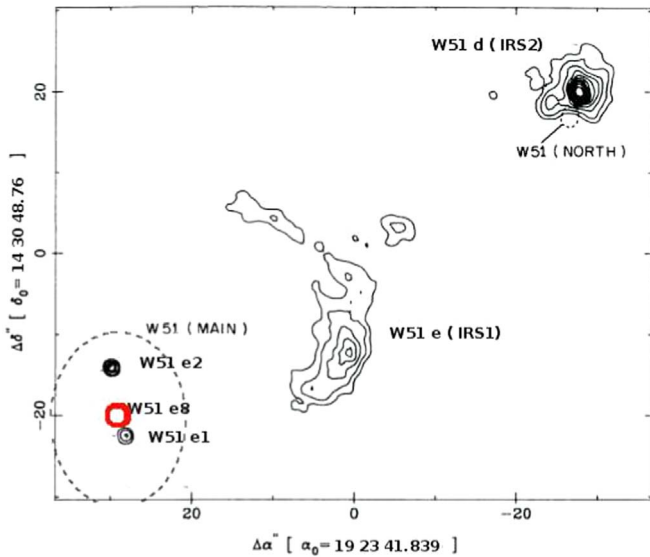


Figure 1. Solid contours: 15 GHz continuum emission in the W51 region, taken from Gaume & Mutel (1987). The red circle shows the hot core e8. The dashed ellipse denotes the region W51 Main.

Therefore, when a new 4 mm wavelength receiver was put into operation at Onsala, we conducted spectral scanning of DR21OH and W51e1/e2 in the 4 mm wavelength range as well. The main purpose of the new survey was to observe molecules whose lines did not fall into the band of the previous survey (DCO⁺, DCN, DNC, etc.), and to check possible detections of molecules made as a result of the previous survey. This article is devoted to W51e1/e2; the results for DR 21 OH will be published separately.

1.1. Region of Massive Star Formation W51e1/e2

The complex of H II regions W51 is located in a giant molecular cloud in the Sagittarius arm at a distance of $5.41^{+0.31}_{-0.28}$ kpc, very close to the tangent point of the Sagittarius spiral arm (Sato et al. 2010), and it consists of four components—A, B, C, and D (Kundu & Velusamy 1967). W51A consists of eight components in the centimeter continuum, designated W51 a – h. The strongest components are e and d (Martin 1972). Scott (1978) identified two closely located radio continuum sources in the vicinity of the component e, designated e1 and e2. The whole region around these two sources is called W51e1/e2. In addition to thermal radio emission, the evidence for an actively ongoing process of star formation in W51A is the presence of bright IR sources, powerful OH, H₂O, and CH₃OH masers, as well as hot cores with rich molecular compositions. The bolometric luminosity of this complex is about $2 \times 10^7 L_{\odot}$, which corresponds to at least 20 O8 stars (Ginsburg et al. 2016). These stars are associated with three sources: W51 Main, W51 IRS1, and W51 IRS2 (also called W51 North; see Figure 1). The IR sources and centers of maser activity W51 Main and W51 IRS2 are associated with the components e1/e2 and d, respectively. These objects are the regions of high-mass star formation in the early stages of evolution. W51 IRS1 is associated with a much more evolved H II region.

Very Large Array observations have shown that W51 Main is a cluster of UC and HC H II regions designated e1 – e8 (Gaume et al. 1993; Mehringer 1994; Zhang & Ho 1997; Goddi et al. 2016). The total bolometric luminosity of the cluster is on

the order of $10^7 L_{\odot}$ (see, e.g., Goddi et al. 2016, and references therein). The brightest HC H II region is e2, which is ionized by an O8 star. It consists of three young stellar objects: W51e2-W, which manifests itself primarily as a hypercompact H II region; W51e2-E, which is the brightest source of dust radiation, as well as the center of a bipolar outflow; and W51e2-NW, which is the center of bipolar outflow detected by the proper motion of H₂O masers. The mass of e2 is $96 M_{\odot}$ (Hernández-Hernández et al. 2014). The most prominent hot cores in W51e1/e2 are associated with e2 and the center of maser activity e8, which is located at a distance of $\sim 6''$ south of e2 and contains $\sim 70 M_{\odot}$ of hot molecular gas. In these two regions, a large number of complex molecules characteristic of hot cores, e.g., HCOOCH₃, CH₃COOH, and CH₃CH₂OH, have been detected. LSR radial velocities of the molecular lines in e2 are about 55–57 km/s, and in e8 about $58\text{--}60 \text{ km s}^{-1}$. The e2 region hosts OH, H₂O, CH₃OH, and CS masers, and the e8 region OH and H₂O masers (Ginsburg & Goddi 2019, and references therein). Goddi et al. (2016) mapped e2 and e8 in metastable lines of ammonia (6,6), (7,7), (9,9), (10,10), and (13,13), with upper-level temperatures E_u/k within the range 408–1691 K. Their maps demonstrate the decrease of the core image diameters with the increase of the upper-level energy. On the other hand, Zhang et al. (1998) found a kinetic temperature as low as ~ 40 K in the outer regions of e2 and e8. Thus, the kinetic temperatures of e2 and e8 vary widely, decreasing with the increase in distance from the protostars.

2. Observations

The observations were carried out with the 20 m radome-enclosed millimeter-wave radio telescope of the Onsala Space Observatory (Sweden) at 68–88 GHz. 20 observation cycles were performed in 2018 April–May. The receiver frontend was a dual-polarization sideband-separating HEMT mixer. A dual-beam switching mode with a switching frequency of 2 Hz and a beam throw of $11'$ in azimuth was applied. The half-power beamwidth at 86 GHz was $43''$. The antenna was pointed toward e2 (R.A. = $19^{\text{h}}23^{\text{m}}43^{\text{s}}.89$, decl. = $14^{\circ}30'36''.4$; J2000). In this case, the whole W51e1/e2 region falls within the antenna beam. Pointing errors were checked using observations of SiO masers at 86 GHz, and found to be within $5''$. The main-beam efficiency varied slightly with frequency and elevation, and was about 0.57 at 86 GHz and an elevation around 65° . The data were calibrated using the chopper-wheel method. The system noise temperature mostly varied within the range $\sim 200\text{--}500$ K, but in the last four observing cycles only it varied from ~ 300 to ~ 1200 K.

A serious problem was the fast radome-induced ripple in the spectral domain, which is more severe in the 4 mm band than the 3 mm band due to the radome material frequency response. This ripple was reduced by using the Path Length Modulator (PLM), which moves the receiver exactly one wavelength along the telescope axis during each integration.

The backend was a fast Fourier transform spectrometer, consisting of four sections. Two sections were used for each plane of polarization, providing an analysis band of 4 GHz. The frequency resolution was 76.294 kHz, corresponding to a velocity resolution of 0.28 km s^{-1} at 83 GHz. At this resolution, the achieved 1σ noise level in the antenna temperature was about 0.012 K at the lower end of the observed frequency range, smoothly decreased while the frequency increased and reached a value of ~ 0.006 K at 70 GHz, then remained almost

constant up to a frequency of 85 GHz, before further increasing with frequency, reaching ~ 0.008 K at the upper boundary of the observed range. During the data reduction, the frequency resolution was smoothed to 0.305 MHz (1.1 km s^{-1} at 83 GHz), so that the rms decreased to 0.003 K for 75% of the band of the survey.

This project served as a pathfinder for the new Bifrost control system, which can conduct observations in a highly automated fashion. Scripts were written that chose science sources with regard to visibility and strived to meet preset observation time targets that varied with tuning, due to the changing atmospheric transmission. Interruptions for pointing and focusing, which also involved automatic retunings, were done based on the time triggers and flag variables, and out of a small number of preselected (at the time) sufficiently strong pointing sources, one was selected by the software based on its current sky position. Observations were halted automatically when weather-related observing conditions increased the system noise above a certain limit (and resumed once the noise decreased again).

Data were reduced using the CLASS software, which is a part of the GILDAS package of Grenoble observatory.

3. Results

The source spectrum covering the frequency range 68–88 GHz is shown in Figure 2. Multiple radio lines of various molecules have been detected, as well as radio recombination lines of hydrogen and helium. The primary identification of the detected lines was carried out using the database of molecular radio lines detected in space (Lovas et al. 2009).⁷ However, many of the detected lines were missing from this database. The identification of these lines was carried out using the WEEDS extension of the CLASS software package. For this purpose, we constructed a model spectrum of W51e1/e2, based on the results of the survey by Kalenskii & Johansson (2010b), performed with the same antenna at a close (partly overlapping) frequency range. When constructing the spectrum, the local thermodynamic equilibrium (LTE) case was assumed. The column densities and excitation temperatures of those molecules whose parameters were determined using rotational diagrams were taken from Table 3 in Kalenskii & Johansson (2010b), and for those molecules whose column densities were obtained from the integrated intensity of a single line, from Table 4 of the same work. In the data reduction process, detected molecules whose lines did not fall into the spectral range of the survey by Kalenskii & Johansson (2010b) were added to the model.

Methylcyanoacetylene ($\text{CH}_3\text{C}_3\text{N}$) was originally detected using spectral-line stacking. The stacking of a large number of spectral lines of the same molecule makes it possible to significantly increase the signal-to-noise ratio and even detect molecules whose individual lines are not seen in the noise. This method is described in, e.g., Loomis et al. (2021). Our work using this method is far from being complete, and its results will be published subsequently. However, we have already detected $\text{CH}_3\text{C}_3\text{N}$, and added it to the model, and after that we could identify several weak lines of this molecule in the observed spectrum.

Often, the newly discovered spectral features turned out to be blends of lines of a large number (>4) of the various

molecules included in the model spectrum. When it was not possible to separate the contributions of these lines, we evaluated the parameters of the entire blend, and instead of writing the molecule name, we wrote Bx in the second column of Table 1, where “x” is the number of lines.⁸ At the same time, lines with an upper-level energy above 2000 K and lines with the value of the Einstein A-coefficient being three or more orders of magnitude lower than that of the strongest line were not taken into account.

In total, 79 molecules and their isotopic species were detected at 4 mm, from simple diatomic and triatomic molecules, such as SO, SiO, and CCH, to complex organic compounds, such as CH_3CN , CH_3OCH_3 , or CH_3COCH_3 . The list of detected molecules is given in Table 2.

A significant portion of the obtained results qualitatively repeats the results of the 3 mm survey. A notable portion of all the detected molecules are those that are typical for hot cores. In particular, we found lines of neutral molecules like HCOOCH_3 , CH_3OCH_3 , $\text{CH}_3\text{CH}_2\text{OH}$, and CH_3COCH_3 , which, according to modern concepts, exist in the gas phase only in hot cores and in hot postshock gas. Another consequence of the fact that we were observing hot gas was the detection of lines from the vibrationally excited levels of, e.g., C_4H and HC_3N , with upper-level temperatures⁹ on the order of several hundred Kelvins. Such lines are likely to be detectable only if they arise from hot gas with a temperature on the order of 100 K or higher.

In addition to the lines of neutral molecules, lines of various molecular ions were found. Some of them (HC^{18}O^+ , HC^{17}O^+ , H^{13}CO^+ , DCO^+ , and HCS^+) are usually present in molecular clouds with large absorption in the visible spectral range A_V .

We could not detect any lines of MgCN or NaCN , molecules that were tentatively found by Kalenskii & Johansson (2010b). Therefore, we believe that the tentative detection of these molecules by Kalenskii & Johansson (2010b) was a result of the incorrect identification of lines wrongly attributed to these molecules. Also, we could not confirm the possible detection of four molecules, HOCH_2COOH , H_2SO_4 , GG’a- $\text{CH}_3\text{CHOHCH}_2\text{OH}$, and 1-C₇H₂, made at 3 mm using spectral-line stacking.

3.1. Rotation Diagrams

For all molecules with four or more spectral lines detected, we have constructed rotation diagrams (RDs) to estimate the rotational temperature and column density of the molecule. These diagrams are shown in Figures 3–5, and the determined parameters with errors are presented in Table 3. For several molecules (shown in Figure 3), there is a clear correlation between the level population and energy, and the rotational temperature is on the order of 100–150 K, roughly in agreement with the temperatures of the hot cores e2 and e8, obtained by Zhang et al. (1998), Remijan et al. (2004), or Goddi et al. (2016). The significant scatterings of the points in some of these diagrams could be caused by deviations of the energy-level populations from the LTE, the heterogeneity of the regions in which the corresponding molecules emit, and/or the high optical depths of some lines. However, it is clear that all these molecules emit mainly in the hot cores e2 and e8.

⁸ We did the same when a specific line is given in the Lovas database at the frequency of the detected spectral feature, but the modeling shows that actually this feature is a blend of lines of several molecules.

⁹ Upper-level energies divided by the Boltzmann constant.

⁷ <https://physics.nist.gov/>

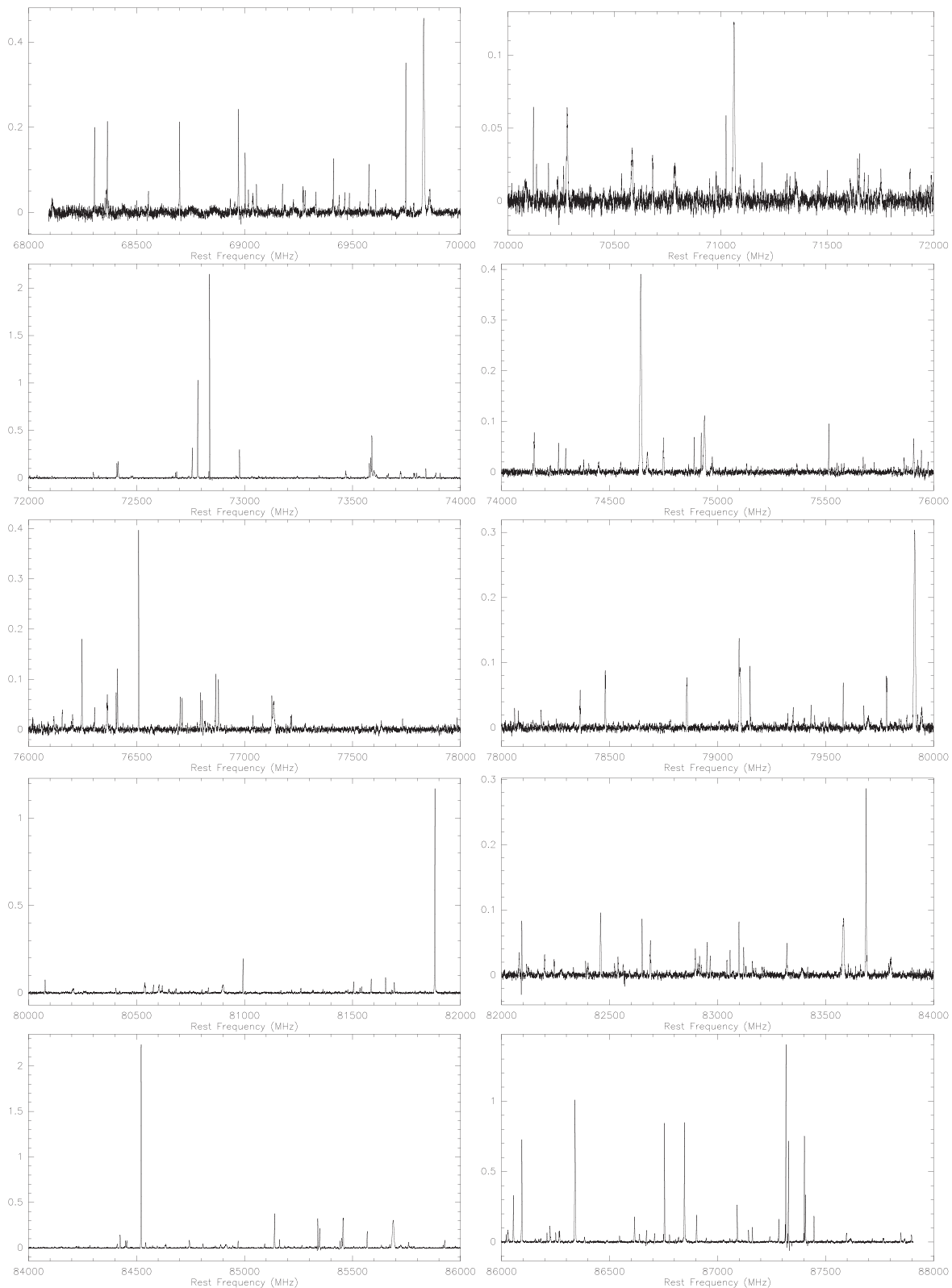


Figure 2. W51e1/e2 spectra in the range of frequencies 68,000–88,000 MHz.

We attribute the molecules CH_3OCH_3 and $\text{CH}_3\text{CH}_2\text{OH}$ to the same group. However, for dimethylether (CH_3OCH_3), the RD constructed using the lines $\Delta J = 0$ (Q-branch) yields T_{rot} of 67 K, and only the RD constructed using the lines $\Delta J = 1$ (R-branch) yields T_{rot} equal to 104 K. This meaningful difference shows that in the case of CH_3OCH_3 , the deviations of the level populations

from the LTE are notable, in which case it is difficult to estimate the source kinetic temperature. The relatively moderate rotational temperature of CH_3OCH_3 , with Q-branch transitions, compared to that of the other hot core molecules in W51e1/e2, may mean that dimethylether sources go beyond the boundaries of hot cores with temperatures $\gtrsim 100$ K and comprise colder regions more

Table 1
Gaussian Parameters of the Detected Lines

Comp.	Frequency (MHz)	Molecule	Transition	$\int T_R dV$ (K km s ⁻¹)	V_{LSR} (km s ⁻¹)	ΔV (km s ⁻¹)	T_R (K)	Notes ^{a,b,c}
0	68305.680	CH ₃ OH	1 _{1,0} – 2 _{0,2} E	3.56(0.06)	56.12(0.07)	8.51(0.15)	0.40	
0	70534.033	H ¹³ CCCN	8–7	0.36(0.04)	56.55(0.41)	9.09(0.91)	0.036	
0	70583.25	RRL	H 70 δ	2.32(0.06)	58.68(0.40)	32.39(0.86)	0.06	
0	70650	U	—	0.12(0.03)	56.87(0.92)	6.81(1.81)	0.016	new; m
0	70678.633	CH ₂	4 _{0,4} – 3 _{1,3} $F = 3 - 2$	0.42(0.04)	58.20(0.35)	11.00(0.88)	0.034	
0	70679.543	CH ₂	4 _{0,4} – 3 _{1,3} $F = 4 - 3$	0.50(0.04)	58.20(0.35)	11.00(0.88)	0.044	
0	70680.720	CH ₂	4 _{0,4} – 3 _{1,3} $F = 5 - 4$	0.62(0.04)	58.20(0.35)	11.00(0.88)	0.054	
0	70784.46	RRL	H 75 ϵ	1.26(0.10)	60.12(1.13)	27.94(2.25)	0.04	
0	70947	U	—	0.22(0.04)	53.99(0.76)	8.40(1.67)	0.024	new
0	70976.795	t-CH ₃ CH ₂ OH	5 _{2,3} – 5 _{1,4}	0.38(0.04)	55.58(0.50)	8.77(1.14)	0.042	bl
0	70979.627	C ₂ H ₅ CN	8 _{0,8} – 7 _{0,7}	0.28(0.04)	57.36(0.56)	7.55(1.38)	0.034	bl
0	71024.781	H ₂ ¹³ CO	1 _{0,1} – 0 _{0,0}	1.02(0.04)	56.27(0.14)	8.28(0.34)	0.12	
0	71062.67	RRL	H 56 β	8.16(0.10)	58.29(0.18)	31.72(0.43)	0.242	
0	71091.63	RRL	He 56 β	0.70(0.06)	57.13(0.96)	23.34(2.43)	0.028	
0	71155.210	¹³ CH ₃ OH	1 ₁ – 2 ₀ E	0.12(0.02)	54.57(0.35)	3.81(0.67)	0.028	new
0	71192.938	OC ³⁴ S	6 – 5	0.34(0.04)	56.64(0.28)	6.25(0.65)	0.05	new
0	71304.063	HCOOCH ₃	17 _{4,13} – 17 _{3,14} E	0.22(0.04)	60.13(0.41)	6.51(1.25)	0.03	new
0	71309.952	HCOOCH ₃	15 _{3,12} – 15 _{2,13} E	0.44(0.04)	54.98(0.44)	10.09(1.01)	0.04	
0	71325	B8	—	0.20(0.02)	59.47(2.70)	7.45(0.54)	0.026	
0	71350	B6	—	0.16(0.02)	57.59(0.43)	5.48(0.98)	0.026	new
0	71357.83	RRL	H 83 η	0.68(0.04)	62.61(0.85)	23.60(1.71)	0.02	
1	71464.138	¹³ CH ₃ CN	4 ₁ – 3 ₁	0.14(0.024)	53.08(0.78)	8.85(2.16)	0.01	m
2	71465.520	¹³ CH ₃ CN	4 ₀ – 3 ₀	—	—	—	—	
0	71500.528	C ₂ H ₅ CN	8 _{2,7} – 7 _{2,6}	0.64(0.04)	58.90(0.28)	11.38(0.65)	0.052	

Notes. Table 1 is published in its entirety in the machine-readable format. A portion is shown here for guidance regarding its form and content. Comp means component of blended lines. Spectral features consisting of two or more unresolved lines are flagged with Comp > 0 and appear consecutively with the primary line used for the radial velocity listed first. 0 = not blended; 1 = the line that is the source of radial velocity in a blended spectral feature; 2 = other line in a blended spectral feature.

^a “new” means that the line is absent from the “List of Recommended Rest Frequencies for Observed Interstellar Molecular Microwave Transitions” (Lovas et al. 2009).

^b “m” means marginal detection.

^c “bl.” means that the line is blended with the neighboring line, but the lines are resolved.

(This table is available in its entirety in machine-readable form.)

Table 2
Molecules Detected in W51e1/e2 in the 4 mm Wavelength Range

Diatomic	NS, Si ¹⁸ O, SiO, ²⁹ SiO, ³⁰ SiO?, SO, ³⁴ SO
Triatomic	CCH, ¹³ CCH, C ¹³ CH, CCS, DCO ⁺ , DCN, DNC, HC ¹⁵ N, H ¹³ C ¹⁵ N, HCO, HDO, HNO?, H ¹³ CO ⁺ , HC ¹⁷ O ⁺ , HC ¹⁸ O ⁺ , HCS ⁺ , H ¹³ CN, HC ¹⁵ N, HN ¹³ C, N ₂ O, OCS, O ¹³ CS, OC ³⁴ S, SO ₂ , ³⁴ SO ₂
Four-atom	C ₃ N, C ₃ S, c- ¹³ CCCH, HNCO, l-C ₃ H, H ₂ CO, H ₂ CS, H ₂ C ³⁴ S?, HOCO ⁺ , NH ₂ D
Five-atom	c-C ₃ H ₂ , C ₄ H, CH ₂ CO, H ¹³ CCCN, HC ¹³ CCN, HCC ¹³ CN, HCCC ¹⁵ N, HCOOH, c-CC ¹³ CH ₂ , H ₂ CCN?
Six-atom	HC ₃ N
Seven-atom	¹³ CH ₃ OH, CH ₃ CN, ¹³ CH ₃ CN, CH ¹³ CN?, CH ₃ ¹⁸ OH, CH ₃ OH, CH ₃ SH, NH ₂ CHO
Eight-atom	C ₆ H, C ₂ H ₃ CN, CH ₃ CHO, c-C ₂ H ₄ O, CH ₃ CCH, CH ₃ NH ₂ , HC ₅ N
Nine-atom	CH ₃ C ₃ N, HCOOCH ₃ , H ₂ C ₃ HNCN?, HCOCH ₂ OH
Ten-atom	CH ₃ CH ₂ OH, CH ₃ OCH ₃ , CH ₃ OHCHO, C ₂ H ₅ CN
Ten-atom	aGg ⁻ -HOCH ₂ CH ₂ OH, CH ₃ COCH ₃

distant from protostars. Note that dimethylether has already been found in even the cold gas phase in the prestellar core L1689B (Bacmann et al. 2012). In the case of ethanol (CH₃CH₂OH), the rotational temperature of the gauche conformer is on the order of 100 K, but Figure 3 shows that it strongly depends on a single point and, therefore, is determined very unreliably (see Table 3). The rotational temperature of the trans conformer is determined much more reliably, and constitutes only 72 K. Therefore, it is possible that ethyl alcohol sources also go beyond the boundaries of hot cores.

The symmetric-top molecule methylacetylene (CH₃CCH) is a good thermometer for interstellar gas, as the rotational temperature obtained from the lines $J_K - (J - 1)_K$ is close to the gas kinetic temperature (Askne et al. 1984). Interferometric observations of the low-mass protostellar binary IRAS 16293-2422 show that the emission of methylacetylene arises in the hot corinos IRAS 16293A and IRAS 16293B, and that the rotational temperature obtained from the CH₃CCH lines is on the order of 100 K (Calcutt et al. 2019). An even higher CH₃CCH temperature, 320 K, has been reported as a result of

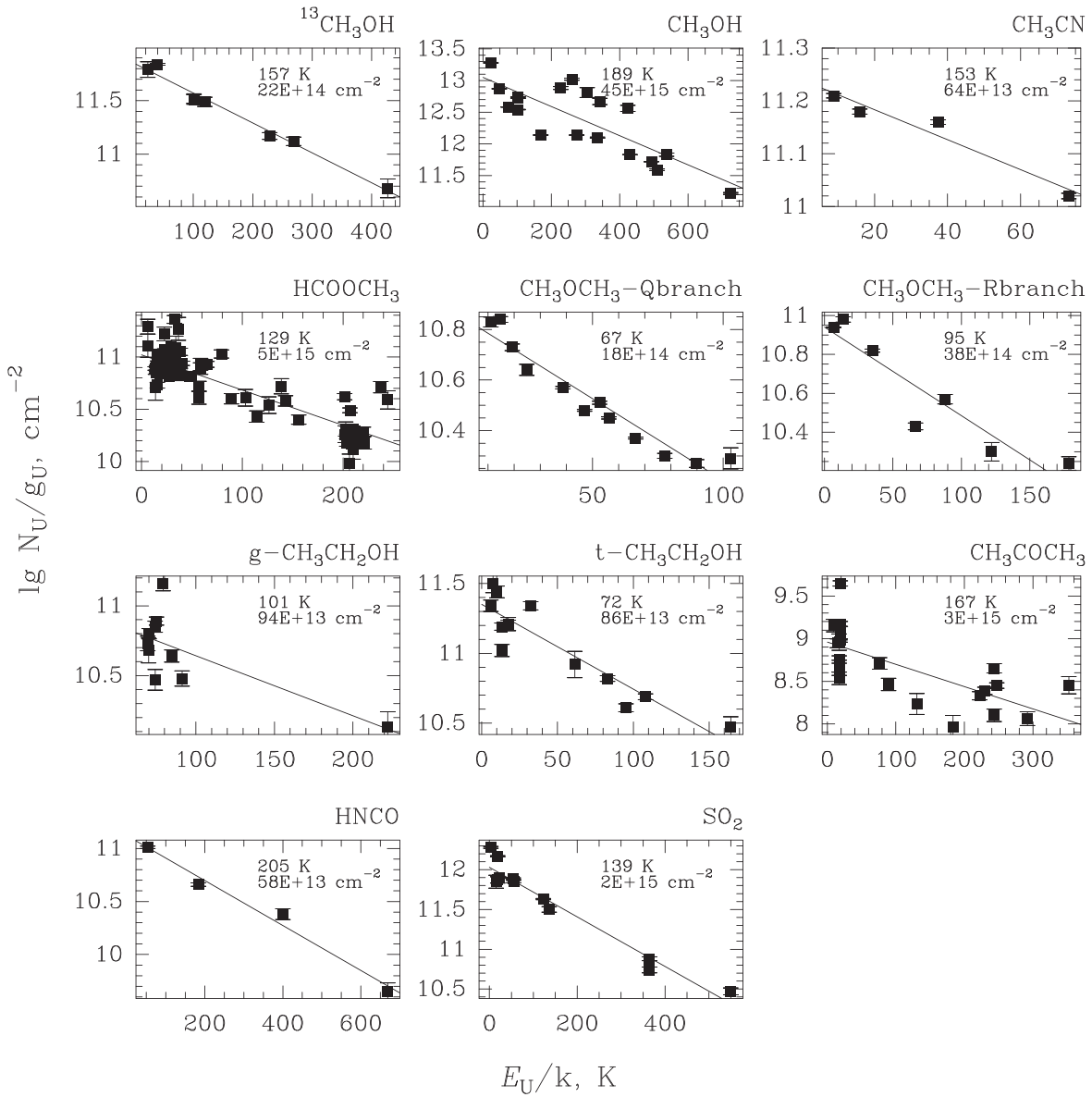


Figure 3. RDs that yield T_{rot} about 100 K or higher.

Atacama Large Millimeter/submillimeter Array observations of the massive star formation region AFGL4176 (Bogelund et al. 2019). However, the rotational temperatures obtained from the CH_3CCH observations with single-dish antennas have proved to be significantly lower, within the range 20–50 K (Askne et al. 1984; Alakoz et al. 2002). This fact shows that in addition to the hot cores, methylacetylene exists in colder gas, and at scales significantly larger than the sizes of hot cores, the contributions of cold regions dominate the radiation of methylacetylene. We obtained a methylacetylene rotational temperature of only 49 K (see Figure 4). Such a low value definitely indicates the presence of colder gas in the observed region and the existence of methylacetylene in this gas.

As for ketene (CH_2CO), its rotational temperature is also fairly low, 68 K. This molecule, in addition to the hot regions, has been observed in cold gas (Irvine et al. 1989; Bacmann et al. 2012), so we believe that the low rotational temperature could appear due to the contribution of cold gas.

The RD for cyanoacetylene (HC_3N) includes both low-energy levels in the ground vibrational state and high-energy levels in the excited vibrational states. The rotational temperature proved to be 95 K. The RD for the next member of the cyanopolyne sequence, cyanodiacetylene (HC_5N), includes only low-energy levels in the ground vibrational state, and the rotational temperature proved to be only 24 K. The difference in the rotational temperatures of the two related molecules can be explained as follows. Suppose that cyanopolyynes are present in both hot cores and cold gas. The transitions between the HC_3N levels in the ground vibrational state are about 50 times stronger than the same HC_5N transitions (see Table 1). Since the transitions between the HC_3N levels in excited vibrational states are very weak, it is not surprising that such HC_5N transitions were not detected due to a lack of sensitivity. Ground-state cyanopolyne lines arise mostly in cold gas, and excited-state lines in hot gas. Therefore, the RD of HC_5N refers to a cold gas, and indicates the presence of a gas with a kinetic temperature of about 24 K. As for HC_3N , this RD is related to a mixture of a cold gas with T_{kin} about 24 K and a hot gas in e2

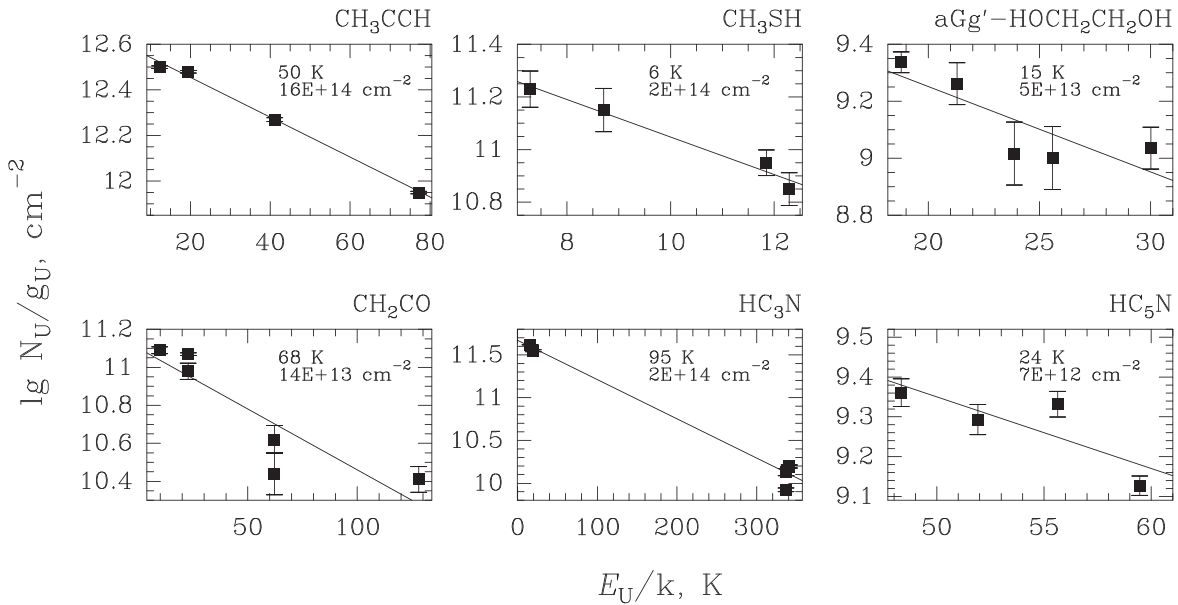


Figure 4. RDs that yield T_{rot} much below 100 K. In addition, we show the HC_3N RD ($T_{\text{rot}} = 95$ K) here, as it is jointly discussed with the HC_5N RD.

and e8. The diagram yields some averaged value of T_{rot} . If we could remove the contribution of the cold gas, the points on the left side of the diagram, which correspond to the lines in the ground state, would go down, and the rotational temperature would increase and would probably become close to the rotational temperatures of SO_2 and CH_3OH , etc.

We believe that for the molecules listed above, RDs yield fairly reasonable rotational temperatures and column densities. However, there are a number of other molecules with more than four lines detected, which are sufficient to construct RDs, but the parameters obtained with these diagrams hardly coincide even approximately with the temperatures of the emitting regions and the molecular column densities.

The RD based on the lines of methyl mercaptan (CH_3SH) shows a small scatter of points, but the rotational temperature turned out to be extremely low, only 6 K (see Figure 4). It is unlikely that the methyl mercaptan source is so cold, as such a low temperature is unusual even for IRDCs, whose temperatures vary between 10 and 20 K (e.g., Pillai et al. 2006), and is extremely unlikely for regions of high-mass star formation at later stages of evolution, such as W51e1/e2. We believe that this temperature can be explained as follows.

The structure of the methyl mercaptan molecule is similar to the structure of the methanol molecule, and the system of the rotational levels and transitions of CH_3SH should be similar to that of methanol. When the gas number density is lower than $\sim 10^7 \text{ cm}^{-3}$, the populations of the rotational levels of methanol differ markedly from the LTE. Based on the modeling of methanol emission by the Large Velocity Gradient method, Kalenskii & Kurtz (2016) analyzed the use of methods based on the LTE assumption—particularly RDs—in the analysis of methanol observations. In particular, they considered the lines $3_K - 2_K$; only $3_K - 2_K$ methyl mercaptan lines were detected in our survey. According to Kalenskii & Kurtz (2016), when the gas number density is insufficient to provide the LTE, the RDs constructed using such lines yield rotational temperatures that are much lower than the kinetic temperature. Moreover, such rotational temperatures depend on the gas number density, rather than on the temperature. We believe that the low T_{rot} value for methyl mercaptan appears for the same reason. Note

that in our survey, we observed completely different lines of CH_3OH and $^{13}\text{CH}_3\text{OH}$, which explains the difference in the methanol and methyl mercaptan rotational temperatures.

Anyway, the RD for methyl mercaptan clearly shows that even a low scatter of points on an RD and small formal errors of T_{rot} and molecular column density do not guarantee that the obtained values represent the source parameters. This happens, in particular, because the LTE condition is often violated in the interstellar medium (ISM). The statement is especially important if a small series of similar lines are used to construct an RD. The safe usage of this method is only possible after careful analysis using statistical equilibrium calculations, such as the one that was carried out for methanol by Kalenskii & Kurtz (2016) or the one for methylacetylene by Askne et al. (1984). Otherwise, the results obtained with RDs can only be trusted if they are supported by other results, which, in the case of well-studied sources such as W51e1/e2, means that they can be trusted with caution only if the results are consistent with the source parameters and the chemistry of the explored molecules.

A low-value rotational temperature was obtained for ethylene glycol ($\text{aGg}'\text{-HOCH}_2\text{CH}_2\text{OH}$; 15 K). Ethylene glycol in the gas phase in the ISM has been found only in hot cores and their counterparts in regions of low-mass star formation (hot corinos); in addition, it has been detected in comets (e.g., Coutens et al. 2018, and references therein). Therefore, we believe that the low rotational temperature can hardly be caused by a contribution of cold gas. Rather, it can be explained by deviations from the LTE.

We built RDs for 11 more molecules (Figure 5), but failed to draw conclusions based on them. Most of these diagrams look peculiar and demonstrate strong scatterings of points. In the cases of HCO , CCH , ^{13}CCH , and C_4H , the ranges of the level energies are extremely small (for the first three of these molecules, we observed different hyperfine components of the same rotational transitions); therefore, even small deviations of level populations from the LTE can lead to significant changes in the slope of the approximating straight line and, therefore, strongly distort the rotational temperature.

The rotational temperatures for $\text{C}_2\text{H}_5\text{CN}$, $\text{C}_2\text{H}_3\text{CN}$, NH_2CHO , and CCH proved to be negative. The RD analysis

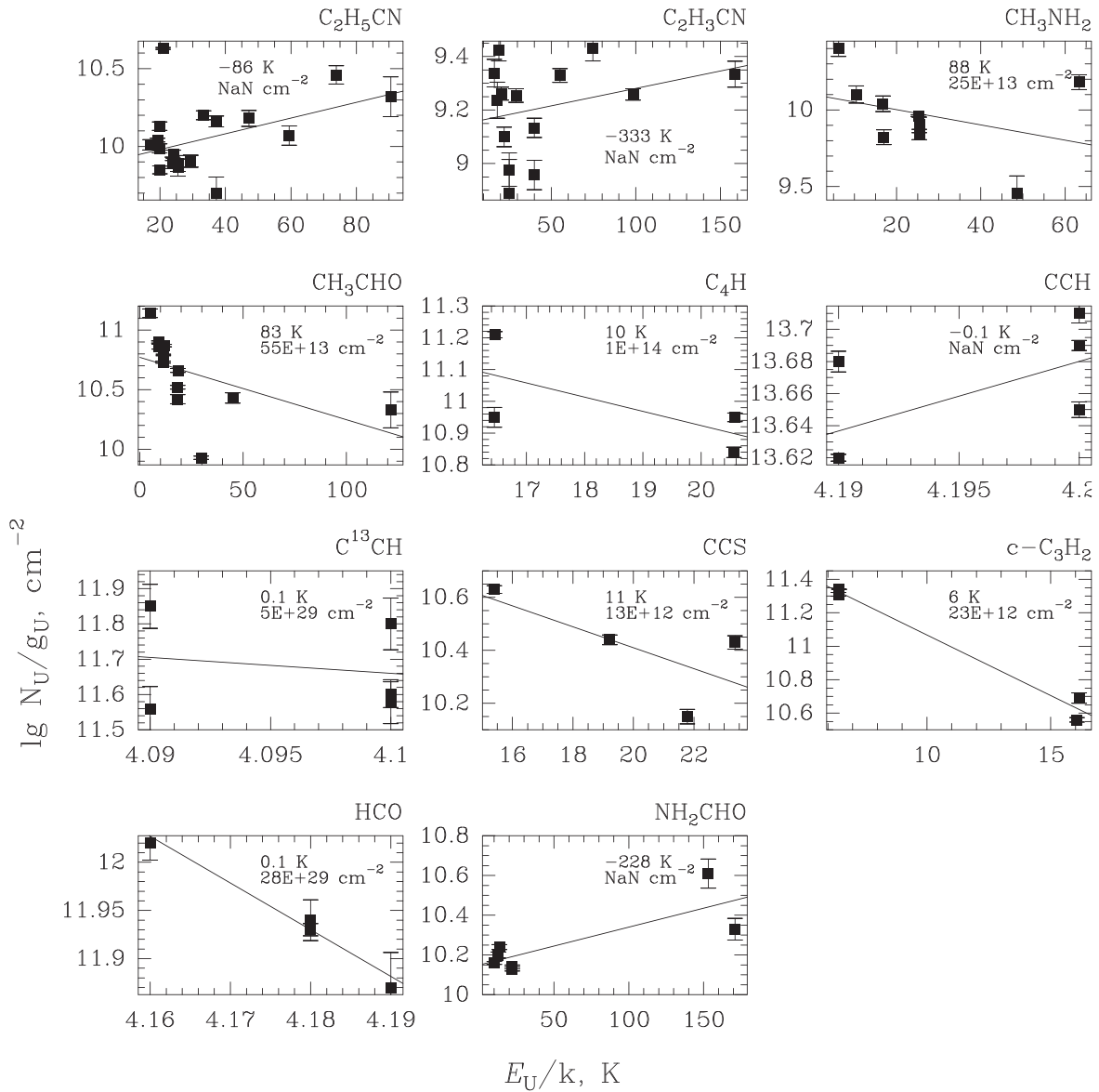


Figure 5. “Peculiar” RDs.

works well for optically thin emission (and for a homogeneous source). If some of the transitions used are optically thick, they will deviate from a straight line in the RD. In such cases, the RD analysis may result in peculiar values for T_{rot} and N , if they are not compensated for. Ginsburg et al. (2016) found that the optical depths of the ammonia lines seen in absorption against the HC H II region W51e2-W vary in the range 10–100. Therefore, it is necessary to understand whether the lines found in this survey are optically thin.

Obviously, a line with $T_R \lesssim 1$ K will be optically thin when the source size is on the order of or larger than the beam size. However, the emission of many molecules arises in hot cores, whose angular sizes in W51e1/e2 are only about 2 arcsec (see Figures 5 and 8 in Ginsburg et al. 2016). One can estimate at what T_R values the lines will be optically thin as follows.

If the lines appear in a thermalized gas with $T_{\text{rot}} \sim 150$ K, the brightness temperature of a line with optical depth $\tau = 1$ will be 95 K. Assuming that the size of the hot cores is about $2''$, we find that the peak main-beam brightness temperature T_R of such a line will be about 0.3. Most of the lines from Table 1 are

significantly weaker, and hence they may be optically thin. This conclusion is supported by the ratios of isotopologue abundances presented in Table 4. The ratios were calculated from the column densities presented in Tables 3 and 5. However, in cases where the rotational temperature was not known, and/or the observed lines of the primary and secondary isotopologues were not the hyperfine components of a single rotational transition, only the lines detected in both the main and the secondary isotopologues were used. The comparisons with the $^{12}\text{C}/^{13}\text{C}$, $^{16}\text{O}/^{18}\text{O}$, $^{32}\text{S}/^{34}\text{S}$, and $^{28}\text{Si}/^{29}\text{Si}$ isotopic ratios show that most of the abundance ratios are consistent with the optical depths of the main isotopologues less than unity. The exceptions are CH_3OH (but this molecule has many lines brighter than 0.3 K), H_2CO , and HC_3N (but the used lines for these molecules are brighter than 0.3 K). The results on OCS are ambiguous: the optical depths of the lines are less than unity, according to the $\text{OCS}/\text{OC}^{34}\text{S}$ ratio, but are close to 3, according to the $\text{OCS}/\text{O}^{13}\text{CS}$ ratio. Anyway, the brightness temperatures of the OCS lines are higher than 0.3 K. Thus, the results of the ratios of isotopologue abundances are consistent

Table 3
Rotational Temperatures and Beam-averaged Column Densities of the Detected Molecules Determined Using RDs

Molecule	T_{rot} (K)	N_{mol} (10^{13} cm^{-2})
$^{13}\text{CH}_3\text{OH}$	157(8)	220(13)
CH_3OH	189(32)	4500(1700)
CH_3CN	153(20)	64(2)
HCOOCH_3	129(9)	500(33)
$\text{CH}_3\text{OCH}_3(\text{Q})$	67(5)	180(14)
$\text{CH}_3\text{OCH}_3(\text{R})$	95(16)	380(64)
$g - \text{CH}_3\text{CH}_2\text{OH}$	101(33)	94(36)
$t - \text{CH}_3\text{CH}_2\text{OH}$	72(9)	86(11)
CH_3COCH_3	167(37)	300(70)
HNCO	205(17)	58(10)
SO_2	139(10)	200(25)
CH_3CCH	50(2)	160(6)
CH_2CO	68(16)	14(4)
HC_3N	95(6)	20(4)
HC_5N	24(10)	0.7(0.9)

Note. The values in parentheses are 1σ errors.

Table 4
Abundance Ratios

Isotope Ratio	Isotopologue Ratio	Abundance Ratio
59^{a} ($^{12}\text{C}/^{13}\text{C}$)	$\text{CCH}/\text{C}^{13}\text{CH}$	45
	$\text{CCH}/^{13}\text{CCH}$	74
	$\text{CH}_3\text{CCH}/^{13}\text{CH}_3\text{CCH}$	43
	$\text{CH}_3\text{CN}/\text{CH}_3^{13}\text{CN}$	40
	$\text{CH}_3\text{CN}/^{13}\text{CH}_3\text{CN}$	119
	$\text{CH}_3\text{OH}/^{13}\text{CH}_3\text{OH}$	20
	$\text{H}_2\text{CO}/\text{H}^{13}\text{CO}$	37^{e}
	$\text{HC}_3\text{N} (v=0)/\text{H}^{13}\text{CCCN}$	36^{e}
	$\text{HC}_3\text{N} (v=0)/\text{HC}^{13}\text{CCN}$	49^{e}
	$\text{HC}_3\text{N} (v=0)/\text{HCC}^{13}\text{CN}$	34^{e}
	$\text{OCS}/\text{O}^{13}\text{CS}$	22^{e}
400^{b} ($^{16}\text{O}/^{18}\text{O}$)	$\text{SiO}/\text{Si}^{18}\text{O}$	$> 81^{\text{e}}$
22^{c} ($^{32}\text{S}/^{34}\text{S}$)	$\text{OCS}/\text{OC}^{34}\text{S}$	16^{e}
	$\text{SO}/^{34}\text{SO}$	16^{e}
	$\text{SO}_2/^{34}\text{SO}_2$	15
19^{d} ($^{28}\text{Si}/^{29}\text{Si}$)	$\text{SiO}/^{29}\text{SiO}$	15^{e}

Notes.

^a Calculated using Equation (5) in Milam et al. (2005)

^b See Figure 2 in Wilson & Rood (1994)

^c Wilson & Rood (1994)

^d Monson et al. (2017)

^e the abundance ratios were determined using only the transitions detected in both the main and secondary isotopologues.

with the assumption that the weak lines ($T_{\text{br}} \lesssim 0.3$ K) detected at 4 mm are usually optically thin.

The lines of any molecule whose RD is presented in Figures 3–5 are on average much weaker than the lines of methanol. In most cases, their brightness temperatures are below 0.3 K. Therefore, one can expect that they are optically thin. Note that even the $^{12}\text{CH}_3\text{OH}$ RD yields a fairly good estimate of the temperature. Therefore, it is reasonable to *assume* that the other believable-looking RDs, constructed from weaker lines, also yield reasonable estimates of the

Table 5
Beam-averaged Column Densities Determined from Individual Lines

Molecule	T_{rot} (K)	N_{mol} (10^{12} cm^{-2})
CCH	49	4689
C^{13}CH	49	104
^{13}CCH	49	63
$c\text{-C}_3\text{H}_2$	49	131
$c\text{-C}_2\text{H}_4\text{O}$	150	107
$c\text{-CC}^{13}\text{CH}_2$	49	6
$l\text{-C}_3\text{H}$	49	14
C_4H	49	111
CCC^{13}CH	49	9
CCS	150	45
CH_2	49	8790
$\text{aGg}'\text{-HOCH}_2\text{CH}_2\text{OH}$	150	341
$^{13}\text{CH}_3\text{CCH}$	49	37
CH_2CN	60	5
$\text{C}_2\text{H}_3\text{CN}$	60	25
$\text{CH}_3^{13}\text{CN}$	153	16
$^{13}\text{CH}_3\text{CN}$	153	5.4
CH_3NC	145	10
CH_2OHCHO	60	11
$\text{C}_2\text{H}_5\text{CN}$	60	93
$\text{CH}_3\text{C}_3\text{N}$	25	$\lesssim 1.6$
CH_3NH_2	60	189
CH_3CHO	60	602
CH_3SH	150	1006
DCO^+	60	2
DCN	150	11
DNC	150	11
HC_3N	24	87
$\text{HC}_3\text{N}, v_7 = 1$	150	99
H^{13}CCCN	24	2
HC^{13}CCN	24	2
HCC^{13}CN	24	3
H_2CO	60	2638
H_2^{13}CO	60	123
H_2CS	60	435
HCO	60	254
HDO	60	78
HNO	60	457
HC^{18}O^+	60	5
HCS^+	150	115
HC^{15}N	25	6
H^{13}CN	25	31
HCOOH	150	562
HN^{13}C	25	13
HOCO^+	49	4
N_2O	150	2866
NH_2CN	150	22
NH_2CHO	150	386
NS	60	396
OCS	150	2130
OC^{34}S	150	130
O^{13}CS	150	95
SiO	150	244
^{29}SiO	150	16
Si^{18}O	150	< 3
SO	150	3595
^{34}SO	150	221
$^{34}\text{SO}_2$	136	136
C_5H^1	150	1

temperatures and beam-averaged column densities. The parameters determined with 15 such RDs are presented in Table 3. However, since the abundances of molecules in the gas phase

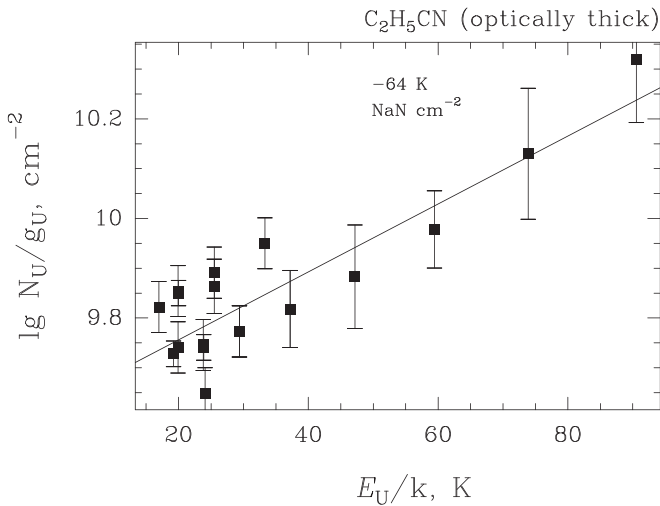


Figure 6. The RD built from optically thick lines of ethylcyanide.

depend on temperature, some molecules probably exist only in the hottest central regions of e2 and e8. The angular sizes of these regions may be much less than $2''$, and even the very faint lines presented in Table 1 may be optically thick. For example, if a source size is $1''$, and its temperature is 200 K, the lines with $T_R \approx 0.1$ K have optical depths of the order of unity. Therefore, it is possible that some peculiar RDs become so due to the large optical depths of the used lines. For example, the RDs for C_2H_5CN and C_2H_3CN show large scatters of points and yield negative rotational temperatures (Figure 5). Figure 6 shows an RD built using the same C_2H_5CN lines that were used to construct the RD in Figure 5, and the brightness temperatures of all the lines were set the same, corresponding to the case of the high optical depth of all lines.¹⁰ The rotational temperature turned out to be negative, and the points show a noticeable scatter, although it is much weaker than the scatter in the corresponding diagram in Figure 5. We believe that the C_2H_5CN emission arises both in cold extended sources and in the hottest central regions of e2 and e8, and that the lines arising in the latter regions are optically thick. In the cold regions, the density can be relatively low, allowing significant deviations from the LTE. This explains the strong scatter of points, corresponding to the low-energy levels. With the increase of the level energy, the contribution of the cold gas decreases, and the radiation of hot regions becomes predominant. The optically thick lines from these regions provide the slopes of the approximating straight lines that correspond to negative temperatures.

To check this scenario, one needs high-resolution maps of W51e1/e2 in the lines of C_2H_5CN and C_2H_3CN . Therefore, further interferometric observations of this source are highly desirable.

The remaining RDs show strong scatters of points that could be caused by deviations from the LTE, source inhomogeneities, errors in determining the parameters of weak lines, as well as contributions of unrecognized weak spectral features to the brightness of the weak lines of the studied molecules. The column densities of the 11 molecules demonstrating peculiar

RDs were estimated using individual lines (see the following section).

3.2. Molecular Column Densities Derived from the Integrated Intensities of Single Lines

If the number of detected lines of a molecule was insufficient to construct an RD, we determined the molecule’s column density from the integrated intensity of a single line. We did the same in those cases where the built RDs proved to be unsuitable for determining the column density. As with the RDs, blended lines were used only when it was possible to reliably separate the individual components. When several lines proved to be suitable for determining the column density of a molecule, we determined it from each of these lines and then averaged the results.

The column density of a molecule can be determined from a single line only when the rotational temperature is known in advance. Often, it was possible to make reasonable a priori assumptions about the value of T_{rot} . For example, the rotational temperature of the cyanopolyynes $H^{13}CCCN$, $HC^{13}CCN$, and $HCC^{13}CN$ was assumed to be 24 K, equal to the T_{rot} of HC_5N . This value was obtained for “cold” cyanopolyynes (see Figure 4). For $CH_3^{13}CN$ and $^{13}CH_3CN$, we used $T_{rot} = 153$ K, equal to that obtained for the main isotopologue CH_3CN . For sulfur-bearing molecules, a hot core temperature of 150 K was taken as T_{rot} , etc. However, for a notable portion of the detected molecules, we could not make reasonable assumptions about the value of T_{rot} . In these cases, we did the following.

The dependence of column density on temperature is described by the well-known formula $N = (N_u/g_u) \cdot Q(T) \cdot \exp(E_u/(kT))$, where the partition function $Q(T)$ is proportional to temperature, in the case of linear molecules, and proportional to $T^{1.5}$, in the case of nonlinear molecules. Based on the results obtained with the RDs, one can assume that the rotational temperatures for different molecules fall within the range ~ 25 –150 K. Taking $T_{rot} = 60$ K, we can underestimate the column density of a nonlinear molecule four times, if the rotational temperature is about 150 K, and overestimate it by a factor of 4 if the rotational temperature is close to 25 K. In the case of linear molecules, the maximum relative error will be 2.5. Therefore, in these cases, we adopt $T_{rot} = 60$ K and consider the relative error of the column density to be no more than four.

The results are shown in Table 5.

Additional results for molecular column densities and abundances will be given in a forthcoming paper devoted to a joint analysis of the data collected at 4 mm in this survey and at 3 mm by Kalenskii & Johansson (2010b).

4. Molecule Formation Mechanisms

The molecular survey of W51e1/e2 provided an inventory of gas-phase molecules, as compiled in Figures 7 and 8. It is important not only to detect these molecules via microwave spectroscopy, but also to discuss potential formation pathways, particularly of complex organic molecules (COMs) and hydrocarbons, along with nitriles, from the bottom up (Abplanalp et al. 2016a; Turner & Kaiser 2020). These formation routes are discussed in this section, first in the context of laboratory experiments elucidating the synthesis of organic molecules in interstellar ices in cold molecular clouds, followed by sublimation into the gas phase in the hot core

¹⁰ This simplified approach was used because it is impossible to reliably model ethylcyanide and vinyl cyanide emission, due to the absence of collisional constants.

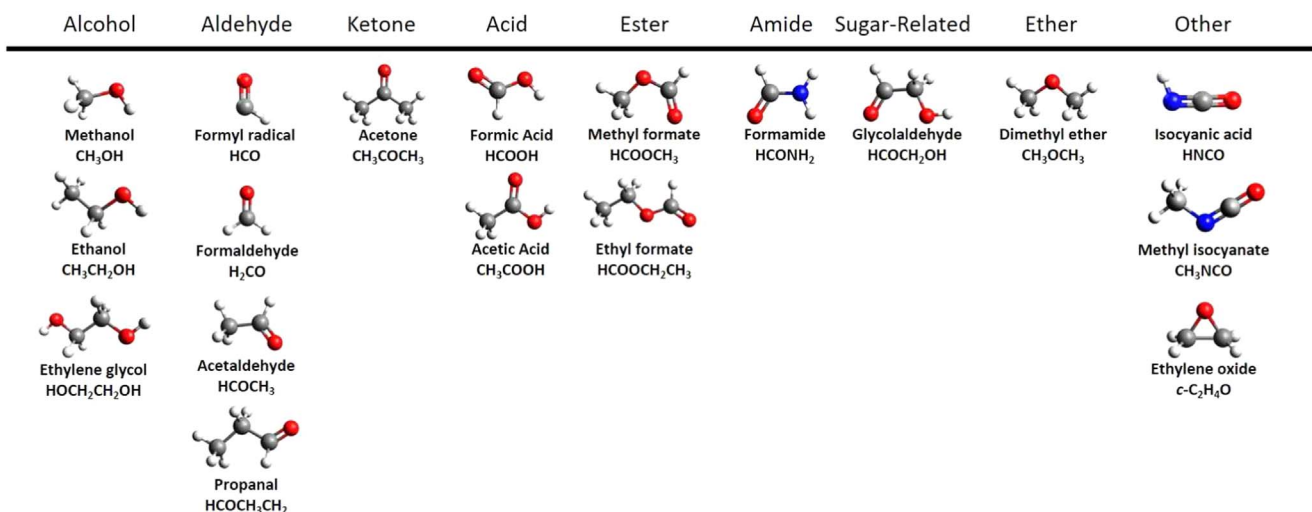


Figure 7. The key COMs detected in the present survey, arranged according to their functional groups.

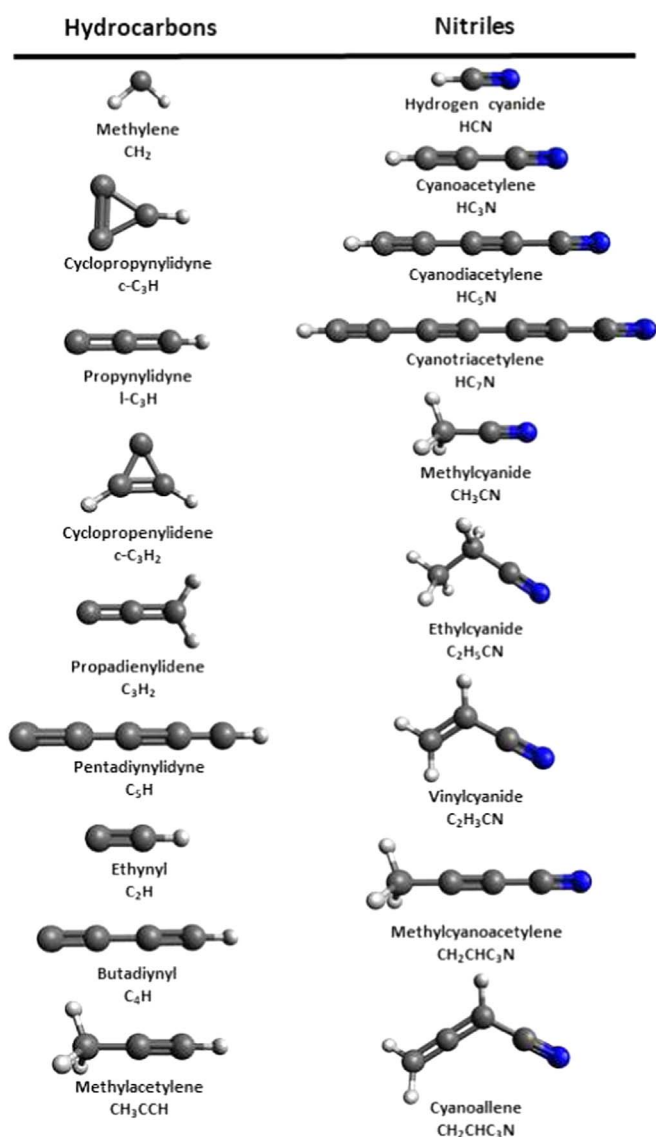
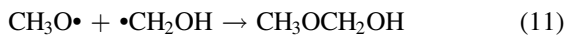
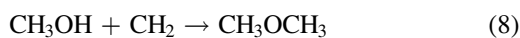
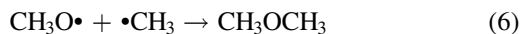
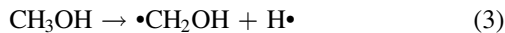
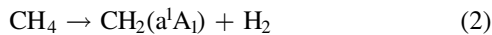


Figure 8. The key hydrocarbon molecules along with the closed-shell nitriles detected in the present survey, arranged according to their functional groups.

stage, as studied through surface science experiments (Figure 7). Thereafter, we discuss the predominant formation of hydrocarbons and their nitriles in the gas phase through bimolecular neutral-neutral reactions (Figure 8). In cold molecular clouds with typical kinetic temperatures near to 10 K, these processes must be exoergic, barrierless, and all transition states must reside lower than the energy of the separated reactants (Kaiser & Mebel 2012). In detail, the surface science experiments replicate the exposure of interstellar analog ices (H₂O, NH₃, CH₄, CO, COS, H₂CO, and CH₃OH) condensed on interstellar grains at 10 K, with energetic electrons as proxies of energetic galactic cosmic rays (GCRs) penetrating even deep inside cold molecular clouds (Bennett et al. 2005b). Once formed inside the ices at 10 K, the transition from the cold molecular cloud to a star-forming region leads to the sublimation of the newly formed molecules from the ices into the gas phase, driven by temperature increases of the ices by up to 300 K. The gas-phase studies exploit crossed molecular beam experiments where the reactants collide under single-collision conditions; this approach guarantees that only primary reaction products are identified (Mebel & Kaiser 2015). To present versatile reaction mechanisms, it is important to rearrange the astronomical inventory of the molecules detected toward W51e1/e2 (Table 2; Figures 7 and 8) according to their chemical functional groups, since the synthesis of molecules with identical functional groups is driven by identical and hence versatile reaction mechanisms (Kaiser & Balucani 2001; Kaiser 2002; Kaiser & Mebel 2002, 2012; Mebel & Kaiser 2015; Abplanalp et al. 2016a; Turner & Kaiser 2020). In Section 4.1, we discuss laboratory experiments exploiting isomer-selective, tunable photoionization; these studies have revealed that COMs, as compiled in Figure 7, can be formed within interstellar ices at 10 K, followed by the sublimation of the new species into the gas phase when the cold cloud transitions to a star-forming region. Thereafter, Section 4.2 provides potential reaction pathways extracted from molecular beam experiments for hydrocarbons and their nitriles in the gas phase.

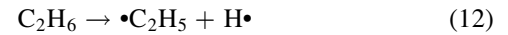
4.1. Formation Routes in Interstellar Ices

Alcohols. Let us start with the documented reaction pathways of alcohols—molecules carrying the R–OH functional group, with R being a hydrocarbon sidechain—and their ether isomers—molecules holding an R–O–R moiety. The reaction pathways to ethanol ($\text{CH}_3\text{CH}_2\text{OH}$) and dimethylether (CH_3OCH_3) were elucidated by Bergantini et al. in methanol (CH_3OH)–methane (CH_4) as well as water (H_2O)–methane (CH_4) ices (Bergantini et al. 2018a, 2017). In detail, methane and methanol can interact with GCR proxies to undergo decomposition via reactions (1) and (2), as well as (3) and (4), respectively. These pathways are endoergic from 4.1 to 5.1 eV, with the reaction endoergicity compensated for by some of the kinetic energy of the impinging GCR proxies, which leads to the methyl radical CH_3 (1) and the singlet carbene $\text{CH}_2(a^1A_1)$ (2), as well as hydroxymethanol CH_2OH (3) and methoxy CH_3O (4). The exoergic formation of ethanol ($\text{CH}_3\text{CH}_2\text{OH}$) and dimethylether (CH_3OCH_3) was found to be driven mainly by the radical–radical recombination pathways (5) and (6) to the less prominent carbene insertion pathways (7) and (8). Likewise, these studies also revealed the formation of three $\text{C}_2\text{H}_6\text{O}_2$ isomers, i.e., ethylene glycol ($\text{HOCH}_2\text{CH}_2\text{OH}$), dimethyl peroxide (CH_3OOCH_3), and methoxymethanol ($\text{CH}_3\text{OCH}_2\text{OH}$), via radical–radical recombination (9)–(11), of which only the diol ethylene glycol ($\text{HOCH}_2\text{CH}_2\text{OH}$) was observed in the present study.



Aldehydes. Aldehydes are defined as organic compounds carrying the formyl moiety ($-\text{CHO}$). In this survey, the three simplest aldehydes—formaldehyde, also known as methanal (H_2CO); acetaldehyde, also called ethanal (CH_3CHO); and propanal ($\text{C}_2\text{H}_5\text{HCO}$)—were detected toward W51e1/e2. Since formaldehyde represents an original component of the interstellar ice inventory (Figure 7), we only present pathways to acetaldehyde and propanal. As extracted from astrophysical ice analog mixtures of carbon monoxide (CO)–methane (CH_4) and carbon monoxide (CO)–ethane (C_2H_6), aldehydes can be formed via the exoergic radical–radical recombination of the formyl radical ($\text{HCO}\bullet$) with any hydrocarbon radical ($\text{R}\bullet$) (14) and (15) (Abplanalp et al. 2016b; Bennett et al. 2005a, 2005b; Turner et al. 2021); formyl itself is formed through the addition of a suprathreshold hydrogen atom to carbon monoxide (13), while hydrocarbon radicals are generated through interactions of GCR proxies with closed-shell hydrocarbons such as methane (1) and ethane (12). Aldehydes act as precursors to their enol tautomers, such as vinylalcohol—also known as hydroxyethylene—($\text{C}_2\text{H}_3\text{OH}$) and cis/trans 1-methyl-2-hydroxyethylene ($(\text{CH}_3)\text{HCCH}(\text{OH})$), which was not identified in the

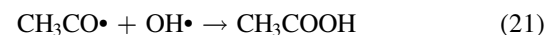
present search (Abplanalp et al. 2016b; Kleimeier et al. 2021a; Kleimeier & Kaiser 2021b). Note that acetaldehyde (CH_3CHO), along with vinylalcohol ($\text{C}_2\text{H}_3\text{OH}$) and propylene oxide ($c\text{-C}_2\text{H}_4\text{O}$), were also identified in the ethylene–carbon dioxide ice mixture exposed to ionizing radiation; in this system, the reaction was initiated by suprathreshold hydrogen atoms and additions to the carbon–carbon double bond, followed by stabilization of the complex and/or isomerization prior to complex stabilization (Bennett et al. 2005b; Bergantini et al. 2018b).



Ketones. Ketones are classified as organic compounds carrying the carbonyl ($\text{C}=\text{O}$) functional group, along with two hydrocarbon moieties at the carbonyl carbon atom (RCOR). In the present survey, the simplest ketone, acetone (or propanone) (CH_3COCH_3), an isomer of propanal ($\text{C}_2\text{H}_5\text{HCO}$), was detected. Methylketones (CH_3COR) can be formed via radical–radical recombination of the acetyl radical ($\text{CH}_3\text{CO}\bullet$) (Bergantini et al. 2018b; Kleimeier et al. 2020a, 2020b, 2020c)—generated via radiolysis of acetaldehyde (16)—and a hydrocarbon radical ($\text{R}\bullet$) via reaction (17) (Maity et al. 2014a). Therefore, acetone (CH_3COCH_3) can be formed via the reaction of the acetyl radical plus methyl (18).

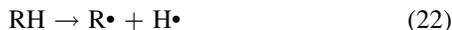


Carboxylic Acids. Carboxylic acids represent organic molecules that contain the carboxyl ($-\text{COOH}$) functional group, with formic acid (HCOOH) and acetic acid (CH_3COOH), as detected in the present survey and by Remijan et al. (2002), being the simplest representatives of this class. In polar, water-rich ices, detailed surface science experiments have revealed that formic acid (HCOOH) can be efficiently formed in carbon monoxide (CO)–water (H_2O) ices through formyl ($\text{HCO}\bullet$)–hydroxyl ($\bullet\text{OH}$) radical–radical reactions (20) within the ices (Bennett et al. 2011); the hydroxyl radical can be generated through GCR proxy interactions with water (19). Acetic acid can be synthesized in polar water (H_2O)–acetaldehyde (CH_3CHO) ices (Kleimeier et al. 2020b). Here, acetyl ($\text{CH}_3\text{CO}\bullet$) radicals formed via radiolysis of acetaldehyde (CH_3CHO) (reaction (16)) undergo radical–radical recombination via reaction (21), with hydroxyl radicals (OH) being generated through radiolysis of water (19).



Acetic acid, along with more complex carboxylic acids with organic sidechains, can also be generated in apolar ices containing carbon dioxide and hydrocarbons (RH) (Bennett & Kaiser 2007a; Zhu et al. 2018). Here, a generic hydrocarbon (RH) can be radiolyzed to the organic radical plus atomic hydrogen (22), followed by the addition of suprathreshold hydrogen to carbon dioxide, forming the hydroxycarbonyl

(HOC•O) species (23). Thereafter, the hydrocarbon radical has been shown to recombine with the hydroxycarbonyl (HOC•O) radical, forming the carboxylic acid (RCOOH) (24). These investigations demonstrate that the polarity of the ice matrix can dramatically alter the underlying formation mechanisms of even simple COMs.



Esters. Esters are defined as organics carrying the RCOOR' moiety, with R and R' resembling organic sidechains. This survey and the previous survey at 3 mm (Kalenskii & Johansson 2010b) have identified methylformic acid ester (HCOOCH₃) and ethylformic acid ester (HCOOC₂H₅). In principle, the formyl radical (HCO•) generated via reaction (13) has been shown to react with the methoxy radical (CH₃O•) formed through radiolysis of methanol (CH₃OH), yielding methylformic acid ester (HCOOCH₃) (reaction (25); Bennett & Kaiser 2007a). It remains to be seen if the versatile route of radical–radical reactions between formyl (HCO•) and an alkoxy (RO•) can be expanded to form ethylformic acid ester (HCOOC₂H₅) via the reaction of formyl with ethoxy (C₂H₅O•) (26). It shall be highlighted that besides the recombination of the formyl radical (HCO•) with the methoxy radical (CH₃O•) to form methylformic acid ester (HCOOCH₃), via reaction (25), a recombination with the hydroxymethyl radical (•CH₂OH) leads to the astronomically observed glycolaldehyde (HCOCH₂OH) (reaction (27); Maity et al. 2015, 2014b; Kleimeier et al. 2021a; Bennett & Kaiser 2007b).



Amides. Amides, such as the observed formamide (HCONH₂), carry an amide (-CONHR) moiety. Detailed experiments have revealed that formamide (HCONH₂) can be formed through radical–radical reaction of the formyl radical (HCO•) with the amino radical (NH₂•) (Jones et al. 2011; reaction (28)), with the latter being formed through radiolysis of ammonia (NH₃) (reaction (29); Zheng et al. 2008). This principle can be also expanded to N-methylformamide (HCONHCH₃) (reaction (30); Frigge et al. 2018), which was not observed in the present survey.



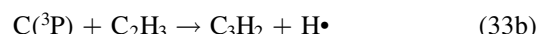
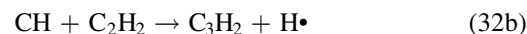
4.2. Formation of Hydrocarbons and Nitriles

C₃H. In this survey, two structural isomers of the doublet tricarbonhydride (C₃H) radicals were observed in the gas phase: linear propynylidyne (l-C₃H) and cyclopropynylidyne (c-C₃H). Crossed molecular beam experiments coupled with electronic structure calculations revealed that both isomers can be formed easily via the barrierless and exoergic neutral–neutral reaction between ground-state carbon atoms (C(³P)) and acetylene (C₂H₂) in the gas phase (reaction (31);

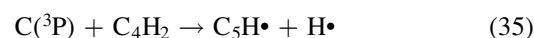
Kaiser et al. 1995, 1996, 1997a, 1997b, 1999; Gu et al. 2007).



C₃H₂. Two structural isomers of tricarbonhydride (C₃H₂) were observed in the present survey: the partially aromatic, cyclic cyclopropenylidene (c-C₃H₂) and the acyclic cumulene-type propadienylidene isomer (C₃H₂). Both molecules hold a C_{2v} point group. Once again, crossed molecular beam studies merged with electronic structure calculations revealed that both isomers can be formed in the gas-phase reactions of the methylidyne radical (CH) with acetylene (C₂H₂) (Maksyutenko et al. 2011; Zhang et al. 2012) and of ground-state carbon atoms (C(³P)) plus the vinyl radical (C₂H₃•) (Nguyen et al. 2001; Wilson et al. 2012; reactions (32) and (33), respectively). It shall be noted that these elementary reactions can also form both tricarbonhydride (C₃H) radicals through the elimination of molecular hydrogen, albeit with lower branching ratios.



C₄H and C₅H. Crossed molecular beam studies revealed that the linear butadiynyl isomer (l-C₄H), which can be considered as an ethynyl-substituted ethynyl (C₂H•) radical, can be formed via the barrierless and exoergic reaction of dicarbon (C₂) with acetylene (C₂H₂) in the gas phase (reaction (34); Gu et al. 2006; Huang et al. 2008). The linear pentadiynylidyne (C₅H) radical was revealed to be the exclusive product of the neutral–neutral reaction between ground-state carbon atoms (C(³P)) and diacetylene (C₄H₂) via reaction (35) (Zhang et al. 2008).

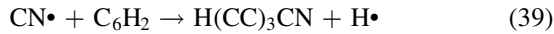
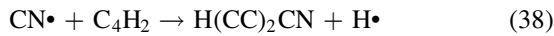


CH₃CCH. The methylacetylene molecule (CH₃CCH) represents a peculiar case, as, to date, no gas-phase reaction involving two neutral reactants has been found to form gas-phase methylacetylene. The microwave inactive allene isomer (H₂CCCH₂), however, can be formed via the neutral–neutral reaction between the methylidyne radical (CH) and ethylene (C₂H₄) (Zhang et al. 2012). However, methylacetylene (CH₃CCH) can be formed in interstellar ices through the radical–radical reaction of a methyl radical (CH₃•) with an ethynyl radical (•C₂H) (reaction (36)), with the latter being formed via interactions of GCR proxies with acetylene (C₂H₂). Once formed, the sublimation in the hot core stage can release methylacetylene into the gas phase (Abplanalp et al. 2018, 2019).



H(CC)_nCN (n = 1-3). Three cyanopolyacetylenes, organic molecules that can be derived from polyacetylene by replacing a hydrogen atom with a cyano group, have been detected in the present survey. Cyanoacetylene, cyanodiacetylene, and cyanotriacetylene can be formed easily via the gas-phase reactions of the cyano radical (CN) with acetylene (C₂H₂), diacetylene

(C₄H₂), and triacetylene (C₆H₂), respectively (37)–(39) (Huang et al. 1999a, 2000; Zhang et al. 2009; Kaiser & Balucani 2001).



C₂H₃CN, CH₃CCCN, and H₂CCC(CN)H. These three nitriles can be formed in analogy to the cyanopolyacetylenes through neutral–neutral reactions of the cyano radical with the corresponding hydrocarbons ethylene (C₂H₄) (Balucani et al. 2000), methylacetylene (CH₃CCH) (Huang et al. 1999b; Balucani et al. 2002), and allene (H₂CCCH₂) (Balucani et al. 2002), as verified via crossed molecular beam studies (reactions (40)–(42)).



CH₃CN and C₂H₅CN. In analogy to methylacetylene, no gas-phase synthesis has been verified so far leading to the formation of methylcyanide (CH₃CN) and ethylcyanide (C₂H₅CN) involving neutral–neutral reactions. However, these saturated nitriles can be formed within interstellar grains via radical–radical recombination of the cyano radical with the methyl and ethyl radicals, respectively, via reactions (43) and (44); it is important to note that this route has not been verified unequivocally in laboratory experiments to date.



5. Conclusion

A spectral-line survey of the massive star formation region W51e1/e2 at 68–88 GHz was conducted with the 20 m radio telescope of the Onsala Space Observatory. An rms sensitivity of 0.003 K was achieved for 75% of the observed band. A number of lines that are absent from the Lovas list of molecular lines observed in space were detected, and most of these were identified. 79 molecules and their isotopic species were detected, from simple diatomic or triatomic molecules, such as SO, SiO, and CCH, to complex organic compounds, such as CH₃OCH₃ or CH₃COCH₃. The list of the detected molecules consists of both the parent species and hydrogen-, carbon-, oxygen-, and nitrogen-related isotopologues. In addition to neutral molecules, various molecular ions were detected. Some of these (HC¹⁸O⁺, H¹³CO⁺, and HCS⁺) usually exist in molecular clouds with high visual extinctions A_V.

A significant number of the detected molecules are typical for hot cores. These include the neutral molecules HCOOCH₃, CH₃CH₂OH, and CH₃COCH₃, which are currently believed to exist in the gas phase only in hot cores and shock-heated gas. Apart from the rotational lines in the ground vibrational state, vibrationally excited lines of several molecules were detected. Among them were C₄H and HC₃N lines, with upper-level temperatures of several hundred Kelvins. Such lines can arise only in hot gas, with temperatures of the order of 100 K or higher. 10 of 15 plausible RDs yield rotational temperatures on the order of, or greater than, 100 K. Therefore, it is obvious that the emissions of many detected molecules arise just in the hot

cores e2 and e8. Unfortunately, we could not separate the contributions of these objects.

Nevertheless, other molecules (CH₃CCH, HC₃N, and CH₂CO) demonstrate lower rotation temperatures, showing that the bulk of their emission arises in colder gas in the vicinity of hot cores.

Potential formation pathways of COMs and hydrocarbons, along with nitriles, are considered. These formation routes are first discussed in the context of laboratory experiments elucidating the synthesis of organic molecules in interstellar ices in cold molecular clouds, followed by sublimation into the gas phase in the hot core stage. Thereafter, we discuss the predominant formation of hydrocarbons and their nitriles in the gas phase through bimolecular neutral–neutral reactions.

The studies at Lebedev Physical Institute were supported by the Ministry of Science and Higher Education of the Russian Federation by grant No. 075-15-2021-597. This paper makes use of NASA’s Astrophysical Data System as well as the following data set: Observed Interstellar Molecular Microwave Transitions (Lovas et al. 2009). The Onsala Space Observatory national research infrastructure is funded through Swedish Research Council grant No. 2017-00648.

Facility: OSO: 20 m (Chalmers University of Technology 20 m Telescope at Onsala Space Observatory).

Software: GILDAS: Grenoble Image and Line Data Analysis Software (Gildas Team, <https://www.iram.fr/IRAMFR/GILDAS>).

ORCID iDs

Sergei. V. Kalenskii  <https://orcid.org/0000-0002-4294-3643>

Ralf I. Kaiser  <https://orcid.org/0000-0002-7233-7206>

A. O. Henrik Olofsson  <https://orcid.org/0000-0003-3125-7346>

References

- Abplanalp, M. J., M. Förstel, M., & Kaiser, R. I. 2016a, *CPL*, **644**, 79
 Abplanalp, M. J., Gozem, S., Krylov, A. I., et al. 2016b, *PNAS*, **113**, 7727
 Abplanalp, M. J., Jones, B. M., & Kaiser, R. I. 2018, *PCCP*, **20**, 5435
 Abplanalp, M. J., Göbi, S., & Kaiser, R. I. 2019, *PCCP*, **21**, 5378
 Alakoz, A. V., Kalenskii, S. V., Promislov, V. G., Johansson, L. E. B., & Winnberg, A. 2002, *ARep*, **46**, 551
 Askne, J., Hoglund, B., Hjalmanson, A., & Irvine, W. M. 1984, *A&A*, **130**, 311
 Bacmann, A., Taquet, V., Faure, A., Kahane, C., & Ceccarelli, C. 2012, *A&A*, **541**, L12
 Balucani, N., Asvany, O., Chang, A. H. H., et al. 2000, *JChPh*, **113**, 8643
 Balucani, N., Asvany, O., Kaiser, R. I., & Osamura, Y. 2002, *JPCA*, **106**, 4301
 Bennett, C. J., Jamieson, C. S., Osamura, Y., & Kaiser, R. I. 2005a, *ApJ*, **624**, 1097
 Bennett, C. J., Osamura, Y., Lebar, M. D., & Kaiser, R. I. 2005b, *ApJ*, **634**, 698
 Bennett, C. J., Hama, T., Kim, Y. S., Kawasaki, M., & Kaiser, R. I. 2011, *ApJ*, **727**, 27
 Bennett, C. J., & Kaiser, R. I. 2007a, *ApJ*, **660**, 1289
 Bennett, C. J., & Kaiser, R. I. 2007b, *ApJ*, **661**, 899
 Bergantini, A., Göbi, S., Abplanalp, M. J., & Kaiser, R. I. 2018a, *ApJ*, **852**, 70
 Bergantini, A., Abplanalp, M. J., Pokhilkov, P., et al. 2018b, *ApJ*, **860**, 108
 Bergantini, A., Maksyutenko, P., & Kaiser, R. I. 2017, *ApJ*, **841**, 96
 Blake, G. A., Sutton, E. C., Masson, C. R., & Phillips, T. G. 1987, *ApJ*, **315**, 621
 Bogelund, E. G., Barr, A. G., Taquet, V., et al. 2019, *A&A*, **628**, 2
 Calcutt, H., Willis, E. R., Jørgensen, J. K., et al. 2019, *A&A*, **631**, A137
 Coutens, A., Viti, S., & Rawlings, J. M. C. 2018, *MNRAS*, **475**, 2016
 Frigge, R., Zhu, C., Turner, A. M., et al. 2018, *ApJ*, **862**, 84
 Gaume, R. A., & Mutel, R. L. 1987, *ApJS*, **65**, 193
 Gaume, R. A., Johnston, K. J., & Wilson, T. L. 1993, *ApJ*, **417**, 645
 Ginsburg, A., Goss, W. M., Goddi, C., et al. 2016, *A&A*, **595**, A27

- Ginsburg, A., & Goddi, C. 2019, *AJ*, **158**, 208
- Goddi, C., Ginsburg, A., & Zhang, Q. 2016, *A&A*, **589**, A44
- Gu, X., Guo, Y., Mebel, A. M., & Kaiser, R. I. 2006, *JPCA*, **110**, 11265
- Gu, X., Guo, Y., Zhang, F., & Kaiser, R. I. 2007, *JPCA*, **111**, 2980
- Hernández-Hernández, V., Zapata, L., Kurtz, S., & Garay, G. 2014, *ApJ*, **786**, 38
- Highberger, J. L., Savage, C., & Ziurys, L. M. 2000, *BAAS*, **32**, 683
- Huang, L. C. L., Lee, Y. T., & Kaiser, R. I. 1999a, *JChPh*, **110**, 7119
- Huang, L. C. L., Balucani, N., Lee, Y. T., Kaiser, R. I., & Osamura, Y. 1999b, *JChPh*, **111**, 2857
- Huang, L. C. L., Asvany, O., Chang, A. H. H., et al. 2000, *JChPh*, **113**, 8656
- Huang, C. Y., Sun, B. J., Kuo, H. H., et al. 2008, *JChPh*, **128**, 244303
- Irvine, W. M., Friberg, P., Kaifu, N., et al. 1989, *ApJ*, **342**, 871
- Jones, B. M., Bennett, C. J., & Kaiser, R. I. 2011, *ApJ*, **734**, 78
- Kaifu, N., Ohishi, M., Kawaguchi, K., et al. 2004, *PASJ*, **56**, 69
- Kaiser, R. I. 2002, *Chem. Rev.*, **102**, 1309
- Kaiser, R. I., Lee, Y. T., & Suits, A. G. 1995, *JChPh*, **103**, 10395
- Kaiser, R. I., Ochsenfeld, C., Head-Gordon, M., Lee, Y. T., & Suits, A. G. 1996, *Sci*, **274**, 1508
- Kaiser, R. I., Ochsenfeld, C., Head-Gordon, M., Lee, Y. T., & Suits, A. G. 1997a, *JChPh*, **106**, 1729
- Kaiser, R. I., Lee, Y. T., Suits, A. G., & Head-Gordon, M. 1997b, *JChPh*, **106**, 4141
- Kaiser, R. I., Ochsenfeld, C., Head-Gordon, M., & Lee, Y. T. 1999, *ApJ*, **510**, 784
- Kaiser, R. I., & Balucani, N. 2001, *Acc. Chem. Res.*, **34**, 699
- Kaiser, R. I., & Mebel, A. M. 2002, *IRPC*, **21**, 307
- Kaiser, R. I., & Mebel, A. M. 2012, *Chem. Soc. Rev.*, **41**, 5490
- Kalenskii, S. V. 2017, arXiv:1708.06829v1
- Kalenskii, S. V., & Johansson, L. E. B. 2010a, *ARep*, **54**, 295
- Kalenskii, S. V., & Johansson, L. E. B. 2010b, *ARep*, **54**, 1084
- Kalenskii, S. V., & Kurtz, S. 2016, *ARep*, **60**, 702
- Kleimeier, N. F., Eckhardt, A. K., & Kaiser, R. I. 2021a, *JACS*, **143**, 14009
- Kleimeier, N. F., & Kaiser, R. I. 2021b, *ChemPhysChem*, **22**, 1229
- Kleimeier, N. F., Eckhardt, A. K., Schreiner, P. R., & Kaiser, R. I. 2020a, *Chem*, **6**, 1
- Kleimeier, N. F., Eckhardt, A. K., & Kaiser, R. I. 2020b, *ApJ*, **901**, 84
- Kleimeier, N. F., Turner, A. M., Fortenberry, R. C., & Kaiser, R. I. 2020c, *ChemPhysChem*, **21**, 1531
- Kundu, M. R., & Velusamy, T. 1967, *AnAp*, **30**, 59
- Loomis, R. A., Burkhardt, A. M., Shingledecker, C. N., et al. 2021, *NatAs*, **5**, 188
- Lovas, F. J., Bass, J. E., Dragoset, K. J., & Olsen, K. J. 2009, NIST Recommended Rest Frequencies for Observed Interstellar Molecular Microwave Transitions, Version 3.0, National Institute of Standards and Technology, Gaithersburg, MD
- Maity, S., Kaiser, R. I., & Jones, B. M. 2014a, *ApJ*, **789**, 36
- Maity, S., Kaiser, R. I., & Jones, B. M. 2014b, *FaDi*, **168**, 485
- Maity, S., Kaiser, R. I., & Jones, B. M. 2015, *PCCP*, **17**, 3081
- Maksyutenko, P., Zhang, F., Gu, X., & Kaiser, R. I. 2011, *PCCP*, **13**, 240
- Martin, A. H. M. 1972, *MNRAS*, **157**, 31
- McGuire, B. A., Burkhardt, A. M., Kalenskii, S. V., et al. 2018, *Sci*, **359**, 202
- McGuire, B. A., Burkhardt, A. M., Loomis, R. A., et al. 2020, *ApJ*, **900L**, 10
- McGuire, B. A., Loomis, R. A., Burkhardt, A. M., et al. 2021, *Sci*, **371**, 1265
- Mebel, A. M., & Kaiser, R. I. 2015, *IRPC*, **34**, 461
- Mehringer, D. M. 1994, *ApJS*, **91**, 713
- Milam, S. N., Savage, C., Brewster, M. A., Ziurys, L. M., & Wyckoff, S. 2005, *ApJ*, **634**, 1126
- Monson, N. N., Morris, M. R., & Young, E. D. 2017, *ApJ*, **839**, 123
- Nguyen, T. L., Mebel, A. M., & Kaiser, R. I. 2001, *JPCA*, **105**, 3284
- Pillai, T., Wyrowski, F., Menten, K. M., & Krugel, E. 2006, *A&A*, **447**, 929
- Remijan, A., Snyder, L. E., Liu, S.-Y., Mehringer, D., & Kuan, Y.-J. 2002, *ApJ*, **576**, 264
- Remijan, A., Sutton, E. C., Snyder, L. E., et al. 2004, *ApJ*, **606**, 917
- Sato, M., Reid, M. J., Brunthaler, A., & Menten, K. M. 2010, *ApJ*, **720**, 1055
- Scott, P. F. 1978, *MNRAS*, **183**, 435
- Turner, A. M., & Kaiser, R. I. 2020, *Acc. Chem. Res.*, **53**, 2791
- Turner, A. M., Bergantini, A., Koutsogiannis, A. S., et al. 2021, *ApJ*, **916**, 74
- Wilson, T. L., & Rood, R. 1994, *ARA&A*, **32**, 191
- Wilson, A. V., Parker, D. S. N., Zhang, F., & Kaiser, R. I. 2012, *PCCP*, **14**, 477
- Zhang, F., Kim, Y. S., Zhou, L., Chang, A. H. H., & Kaiser, R. I. 2008, *JChPh*, **129**, 134313
- Zhang, F., Kim, S., Kaiser, R. I., Jamal, A., & Mebel, A. M. 2009, *JChPh*, **130**, 234308
- Zhang, F., Maksyutenko, P., & Kaiser, R. I. 2012, *PCCP*, **14**, 529
- Zhang, Q., & Ho, P. T. P. 1997, *ApJ*, **488**, 241
- Zhang, Q., Ho, P. T. P., & Ohashi, N. 1998, *ApJ*, **494**, 636
- Zheng, W., Jewitt, D. C., Osamura, Y., & Kaiser, R. I. 2008, *ApJ*, **674**, 1242
- Zhu, C., Turner, A. M., Abplanalp, M. J., & Kaiser, R. I. 2018, *ApJS*, **234**, 15
- Ziurys, L. M., Apponi, A. J., Guelin, M., & Cernicharo, J. 1995, *ApJ*, **445**, L47